Computer simulations of excess electron transport in neon

Francesco Ancilotto and Flavio Toigo
Dipartimento di Fisica "G. Galilei," Università di Padova, Via Marzolo 8, I-35131 Padova, Italy
(Received 17 September 1991)

The behavior of excess electrons in neon gas in a wide range of densities is investigated using molecular-dynamics simulations with a parameter-free interparticle potential. A realistic pseudopotential reproducing the measured electron-Ne low-energy scattering properties is used. A transition from quasi-free behavior to a localized regime where the electron is trapped in a bubblelike cavity is observed as the density is increased beyond a value that is close to the experimental one. The calculated electron mobilities in a wide range of densities are also found to be in reasonable agreement with the experimental data.

PACS number(s): 51.50.+v 71.55.Jv 34.80.−i

I. INTRODUCTION

It is well known that in most molecular liquids the ground state of an excess electron has a localized character, the electron being trapped in a bubblelike cavity in the solvent [1]. The driving force for the localization is the long-range anisotropic interaction between the electron and the solvent dipoles, which is sufficient to overcome the increase in kinetic energy due to localization. In nonpolar liquids a localized bubble state of an excess electron is also expected to be stable provided that the electron-atom repulsion is sufficiently strong [2]. In this case the stabilization effect comes as a consequence of the balance between the electron-atom short-range repulsion, the increased electron kinetic energy due to localization, and the free energy required to form the liquid-bubble interface. The mobility of the electron under these conditions is expected to be rather low because a large number of atoms in the fluid must be displaced for the cavity to move. In He, for instance, as the gas density increases beyond a certain value, the electron mobility is observed to drop much faster than the classical rate, as the electron becomes localized [3].

Evidence for localized excess electron states in noble-gas liquids has been found long ago. However, only very recently experimental evidence for localization of excess electrons in Ne gas at moderately high densities has been collected [4,5]. In particular, measurements of the excess electron mobility at low temperature ($T \sim 46-48$ K) and in a wide range of gas densities show that a transition from quasifree to localized electron states, signaled by a dramatic drop in the zero-field electron mobility, takes place at neon densities between 1.3 and 1.5×10^{22} cm^{-3}.

The low-density mobility data, where quasifree behavior of the electrons is assumed, can be explained [4,5] on the basis of multiple scattering theory, where the mobility is given by

$$\mu_e = \frac{4e}{3h} S(0)^{-1} \lambda \lambda^* \exp(-\pi^{-1/2}\lambda/\lambda^*). \quad (1)$$

Here $\lambda = h(2\pi m k_B T)^{-1/2}$, $S(0) = \rho k_B T \chi_T$ is the long-wavelength part of the fluid structure factor, ρ and χ_T being the number density and the isothermal compressibility of the fluid, respectively, and

$$\lambda^* = (\rho\sigma^*)^{-1} = (k_B T)^{-2} \int_0^\infty \frac{\varepsilon e^{-\varepsilon/k_B T}}{\rho\sigma(\varepsilon_0+\varepsilon)} d\varepsilon \quad (2)$$

is the energy-averaged electron mean free path. In Ref. [6] one can find an analytic expression for the energy dependence of the total scattering cross section $\sigma(\varepsilon)$ appearing in (2) which fits the experimental data to high accuracy. Note that in (2) σ has to be evaluated at the shifted energy $\varepsilon + \varepsilon_0$ [5]. The energy shift ε_0, which depends on the density ρ of scatterers [5], can be easily calculated explicitly if, for instance, an ordered array of scatterers is assumed [7]. In this case $\varepsilon = k^2/2m^*$ (m^* being a suitable scalar effective mass) is the free particle energy term, while the zero-point energy $\varepsilon_0 \equiv k_0^2/2m^*$ can be obtained by matching the electron wave function with its asymptotic expression $\phi(r) \sim \sin[kr+\delta_0(k)]/kr$ on the surface of a Wigner-Seitz sphere (of volume $\frac{4}{3}\pi r_s^3 = \rho^{-1}$) centered on each atom, i.e., k_0 is determined by solving the equation $\tan[k_0 r_s + \delta_0(k_0)] = k_0 r_s$. Even such a simple estimate for $\varepsilon_0(\rho)$, when inserted in (2), is found to give a good fit to the mobility data in the low-density, delocalized regime [5].

On the high-density side, however, where the drop in the mobility is observed, a conclusive theoretical description of the behavior of the excess electron is still lacking. Recent calculations [7], based on a model local-density functional coupled with Wigner-Seitz boundary conditions, show that spontaneous electron self-trapping in a bubble occurs at densities larger than $\rho_0 \sim 1.5 \times 10^{22}$ cm^{-3}, in agreement with experiments [5]. However, the disagreement between theoretical and experimental values for the mobility in the range of densities $\rho > \rho_0$, where localization occurs, is substantial, the calculated mobilities being much lower than experimentally observed.

In the attempt to characterize theoretically the behavior of excess electrons in neon at different densities and to give a microscopic description of the localization process, we have performed a series of computer simulations of

such a system, both in the density range where quasifree behavior is observed and at higher densities where localization is expected.

The following section contains a brief description of the method used, while in Sec. III we give a detailed derivation of an essential ingredients of our simulations, i.e., the electron-Ne interaction potential. In Sec. IV we summarize the main results of our calculations. Few concluding remarks form the subject of Sec. V.

II. METHOD

A number of numerical techniques can be used to simulate on a computer the behavior of electrons in a disordered atomic system [8]. Among them, molecular dynamics (MD) is best suited to investigate time-dependent phenomena like diffusion or transport. Here we use a method introduced a few years ago by Car and Parrinello [9] to study the physical properties of condensed-matter systems (i.e., a many-body system of electrons plus ion cores), which allows us to perform molecular dynamics with a *parameter-free* interatomic potential.

This method combines the practical advantages of standard MD techniques for the calculation of the statistical properties of a classical system of particles with the first-principles treatment of interatomic forces due to the quantum electronic system, as provided by density-functional theory. A detailed description of the Car-Parrinello method can be found in Ref. [10], together with a number of applications to complex condensed-matter systems. We only recall here the basic equations of this method, as applied to the simpler system that we are facing, i.e., a *single* electron interacting with N classical atoms contained in a volume Ω.

A fictitious dynamical system described by two sets of *classical* degrees of freedom, the atomic spatial coordinates $\{\mathbf{R}_I\}$ $(I = 1, \ldots, N)$ and the electron wave function $\Psi(\mathbf{r})$, is introduced and the following coupled equations of motion are derived:

$$\mu\ddot{\Psi}(\mathbf{r},t) = -\frac{\delta E}{\delta \Psi^*} + \lambda\Psi(\mathbf{r},t), \tag{3a}$$

$$M_I\ddot{\mathbf{R}}_\mathbf{I} = -\nabla_{R_I} E. \tag{3b}$$

The total energy functional E is given by

$$E[\Psi,\{\mathbf{R}_I\}] = -\tfrac{1}{2}\int_\Omega \Psi^*\nabla^2\Psi\, d\mathbf{r} + \int_\Omega \sum_I V(|\mathbf{r}-\mathbf{R}_I|)|\Psi(\mathbf{r})|^2 d\mathbf{r} + \tfrac{1}{2}\sum_{I\neq J} V_{a\text{-}a}(|\mathbf{R}_I-\mathbf{R}_J|). \tag{4}$$

Here $V(|\mathbf{r}-\mathbf{R}_I|)$ is the potential acting on the electron due to an atom at $\mathbf{R}_I$ and $V_{a\text{-}a}$ is the atom-atom pair potential. The constant μ in Eq. (3a) represents a fictitious mass associated with the electronic "degree of freedom" Ψ, while λ is a Lagrange multiplier that imposes the normalization constraint on the electron wave function. If Ψ is the ground-state wave function, Ψ_0, for a given atomic configuration $\{\mathbf{R}_I^0\}$, and if the fictitious mass μ is chosen so that $\mu \ll M_I$, thus preventing transfer of energy from the atoms to the electron over long periods of simulation, then the trajectories $\{\mathbf{R}_I(t)\}$ obtained from the above equations of motion follow very closely the true atomic trajectories for the physical system [10]. These "quasi-adiabatic" atomic trajectories can be used to extract statistical averages as temporal averages over the observation time. A temperature T can be defined in terms of the mean classical kinetic energy of the atoms and can be varied by simply rescaling the atomic velocities $\{\dot{\mathbf{R}}_I\}$. As long as the "false" kinetic energy associated with the electronic degree of freedom $K_e \equiv (\mu/2)\int|\dot{\Psi}(\mathbf{r})|^2\, d\mathbf{r}$ remains negligible with respect to E and to the total atomic kinetic energy $K_I = \frac{1}{2}\sum_I M_I\dot{\mathbf{R}}_I^2$, then the sum $K_I + E$ is almost constant during the temporal evolution of the system. This provides a useful check that during the run no transfer of energy takes place from the atoms to the electron.

As described in detail in the following section, we derived a realistic electron-atom interaction V to be used in (4) in the form of a smooth pseudopotential, constructed in such a way as to reproduce the scattering properties of Ne in the range of energies of interest here.

The other basic ingredient appearing in the equations of motion (3) is the atom-atom pair potential $V_{a\text{-}a}$. For the purpose of representing both the short-range repulsion and the long-range van der Waals attraction between pairs of rare-gas atoms the following model potential has been proposed [11]:

$$V_{a\text{-}a}(R) = A\exp(-bR) - \sum_{n>2} f_{2n}(b)\frac{C_{2n}}{R^{2n}}. \tag{5}$$

Five essential parameters are required to completely specify the potential (5) for a given rare-gas atomic pair, and they are listed in Ref. [12]. The A, b parameters of the repulsive Born-Mayer term are derived from a fit to experimental results, while the dispersion coefficients C_6, C_8, C_{10} can be obtained from perturbation theory [11]. The remaining C_{2n}'s are derived by a recursion relation. The f_{2n} are given universal functions [11].

The potential function (5) has been tested successfully against the best experimental and theoretical *ab initio* results for the He_2 and Ar_2 dimers as well as for a number of heteronuclear dimers [12]. We have tested the above potential for Ne-Ne pairs in a fluid environment by performing a standard MD simulation for a system of classical particles interacting through (5). To simulate an infinite system we used periodic boundary conditions on the surface of a cubic box of side L containing N atoms. In our test we took $N = 219$ and $L = 36$ a.u., corresponding to a density $\rho = N/L^3 = 3.17 \times 10^{22}$ cm^{-3}. Starting from a randomly chosen initial configuration $\{\mathbf{R}_I\}$ of the N particles, we let the system equilibrate for about ~ 2 ps while its temperature was kept around $T \sim 35$ K by periodically rescaling the atomic velocities. After this equilibration run, we made a "production" run of about ~ 7 ps. From the atomic trajectories generated during this run, we computed the radial pair correlation function

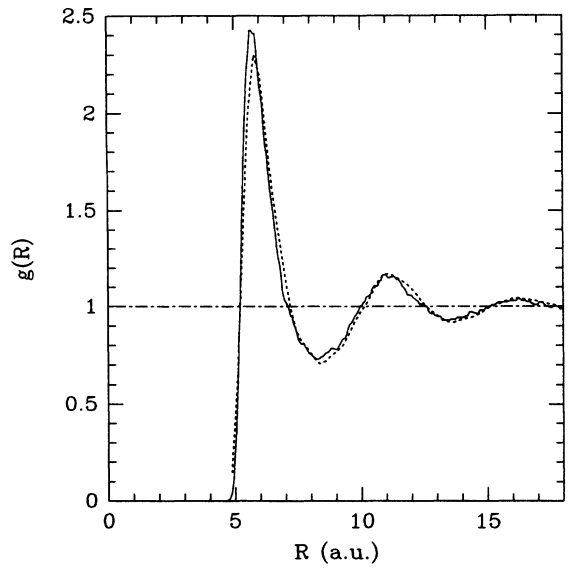

FIG. 1. Radial distribution function $g(R)$ of liquid neon at $T = 35$ K and $\rho = 3.17 \times 10^{22}\,\mathrm{cm}^{-3}$. Solid line, calculated from classical MD simulations using the model pair potential of Ref. [11] [see Eq. (5) in the text]. Dotted line, experimental results of de Graaf and Mozer [13], as analyzed by Raveche and Mountain [14].

$g(R) = (4\pi R^2 \rho N)^{-1} \sum_{I \neq J} < \delta(\mathbf{R} - |\mathbf{R}_I - \mathbf{R}_J|) >$.

Our calculated $g(R)$ is compared in Fig. 1 with the experimental results from neutron scattering experiments in liquid Ne at the same temperature and density [13, 14]. It appears from Fig. 1 that a good overall agreement with the experimental pair-correlation function is attained, the main difference being in the height of the first peak of $g(R)$, which in our calculations is slightly higher than in the experimental curve. This is a manifestation of quantum effects which are displayed by Ne at liquid-state temperatures [15]: the mild suppression in the height of the experimental peak reflects the occurrence of tunneling of Ne atoms through the (classically forbidden) shell of first neighbors. These effects are obviously not accounted for in our purely classical simulations. They are however quite small [15] and are expected to be negligible at the lower densities and at the higher temperature of our excess electron calculations described in the following sections.

III. MODELING THE ELECTRON-NEON INTERACTION

Pseudopotentials greatly simplify electronic-structure calculations by eliminating the need to include deep atomic core states and the strong potential responsible for binding them; i.e., the electron-ion interaction potential is replaced by a weaker effective potential acting only on the valence electrons. In particular, the widely used norm-conserving pseudopotentials (NCPP) calculated from *ab initio* self-consistent potentials in the local-density approximation (LDA) produce pseudoatomic valence wave functions which converge identically to the real wave functions beyond a chosen core radius. This property guarantees optimum transferability of NCPP among different chemical environments [16]. Recently, a class of "generalized" NCPP [17] have been computed from LDA all-electron atom potentials at arbitrary energies, rather than at bound-state energies only, as in previous methods [16]. This results in more flexible NCPP which may be used to treat certain "problem" atoms where previous NCPP proved to be inadequate [17]. These pseudopotentials were also claimed to be able to reproduce the scattering properties of closed-shell atoms.

However, as we tried to apply the generalized NCPP scheme of Ref. [17] to neon, we found that the resulting pseudopotential failed completely to reproduce the scattering properties of the atom at energies in the continuum. The calculated scattering phase shifts δ_l ($l = 0, 1, 2, \ldots$) turned out to be completely wrong when compared to the experimental results [6]. In particular, the predicted scattering length $a_s \equiv -\lim_{k \to 0} tg(\delta_0)/k$ was found to be exceedingly large with respect to the experimental value $a_s^{\mathrm{expt}} = 0.213$ a.u. [6].

The reason for this failure is that LDA is unable to reproduce the long-range polarization effects which describe the electron–closed-shell-atom interaction at large electron-atom distances, and which are essential in determining the atom scattering properties. We thus proceeded to construct a realistic potential in which these polarization effects were included from the start.

An accurate description of electron scattering from closed-shell atoms requires an accurate treatment of both exchange and correlation effects. At large electron-atom distances, the correlation potential takes the form of a dipole polarization term $V_c(r) \sim -\alpha_d/2r^4$, α_d being the electric polarizability of the atom. The above form applies only in the asymptotic limit $r \to \infty$, whereas its proper form at small r is not known.

Among rare-gas atoms, the importance of dynamical polarization of inner-shell electrons is greater for Ne, due to its exceedingly small scattering length [6]. For this reason accurate calculations of its properties from first principles are extremely difficult. Recently, very accurate *ab initio* calculations of the low-energy scattering properties of Ne have been performed, based on a multiconfiguration Hartree-Fock method [18]. The resulting scattering length and phase shifts agree almost perfectly with the experiments [6]. The method of Ref. [18], however, is not suited to be implemented in a molecular-dynamics computer simulation, where an explicit representation of the electron-atom interaction potential is desirable.

In order to construct a realistic electron-Ne interaction potential, we partially followed the prescription of Ref. [19], where a procedure to construct a model potential containing the essential physics of electron-closed shell atom interaction is given. Although not completely *ab initio*, this model potential does not contain any semiempirical adjustable parameter, the only input being the electron charge density of the unperturbed atom (calculated, e.g., using the Hartree-Fock method) and the polarizability α_d of the atom.

The full electron-atom interaction potential can be

written as $V(r) = V_s(r) + V_x(r) + V_c(r)$. The static potential V_s, due to the Coulomb interaction of the electron with an N-electron closed-shell atom, can be written as [19] $V_s = -[Z - y_0(r)]/r$, where Z is the atomic number and

$$y_0(r) = \sum_{i=1}^{N} \left(\int_0^r P_i^2(r')dr' + r \int_r^\infty \frac{P_i^2(r')}{r'} dr' \right). \quad (6)$$

For the bound electronic orbitals P_i appearing in (6) we took the analytic Hartree-Fock functions of Clementi and Roetti [20]. The electron density is given in terms of these orbitals by $n_e(r) = (1/4\pi r^2) \sum_{i=1}^{N} P_i^2(r)$.

An explicit form for the exchange potential V_x can be derived from the free-electron-gas (FEG) exchange potential

$$V_x^{(\mathrm{FEG})} = -\frac{2}{\pi} K_F \left(\frac{1}{2} + \frac{1-\eta^2}{4\eta} \ln \left| \frac{1+\eta}{1-\eta} \right| \right) \quad (7)$$

with $\eta = K(\mathbf{r})/K_F(\mathbf{r})$ defined in terms of a local momentum $K(\mathbf{r})$ and the local Fermi momentum $K_F(\mathbf{r}) = [3\pi^2 n_e(\mathbf{r})]^{1/3}$. A modification of the above expression is required for the case of unbound electron scattering [21], i.e., a shift in the zero of the energy and hence of the local momentum $K(\mathbf{r})$ of the incident electron: $K^2(\mathbf{r}) = K_F^2(\mathbf{r}) + 2I + k^2$, where I is the ionization potential of the target atom and $k^2/2$ is the kinetic energy of the incident electron.

At short distances the correlation potential $V_c \sim V_c^{\mathrm{SR}}$ is adequately described by using the standard parametrization [22] of the Green-function Monte Carlo results of Ceperley and Alder [23]. At large distances $V_c \sim V_c^{\mathrm{LR}} \sim -\alpha_d/2r^4$ ($\alpha_d^{\mathrm{Ne}} = 2.66 a_0^3$). The correlation potential V_c is obtained everywhere in the simplest way [19] by continuously joining the short- and long-range terms V_c^{SR}, V_c^{LR} at the point r_c where the two cross:

$$V_c(r) = \begin{cases} V_c^{\mathrm{SR}} & (r \le r_c) \\ V_c^{\mathrm{LR}} & (r > r_c). \end{cases} \quad (8)$$

With the full potential $V(r)$ constructed in the way described above, we numerically integrate the radial partial-wave Schrödinger equation in the range of energies $0 < E < 2$ eV (which is the energy range of interest in the present calculations), and we compute the scattering phase shifts δ_l ($l = 0, 1, 2$) for the lth partial wave by matching the numerical wave function with its proper asymptotic form. The agreement with the experimental values for δ_l [6] turns out to be rather qualitative, the discrepancy between theory and experiment increasing with the energy and being as large as $\sim 15\%$ at $E = 2$ eV. Moreover, the calculated scattering length a_s is found to be twice as large as the experimental value $a_s^{\mathrm{expt}} = 0.213$ a.u. [6]. A much better agreement with experiments can be achieved, however, by considering the energy shift $k_0^2 \equiv 2I + k^2$ appearing in the modified exchange potential (7) as an (energy-independent) adjustable parameter, tuned in order to give the best fit to the observed phase shifts. By using the value $k_0^2 = 0.82$ a.u. an excellent overall fit with the measured phase shifts is obtained and the corresponding calculated scattering length is $a_s = 0.205$ a.u., very close to the experimental value.

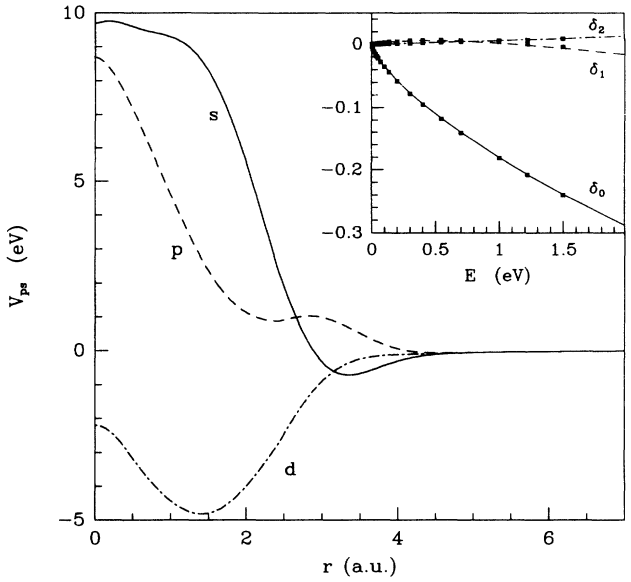

FIG. 2. Neutral-Ne pseudopotential. The $l = 0, 1, 2$ angular momentum components, labeled with s, p, d, respectively, are shown. The inset shows the scattering phase shifts δ_0, δ_1, δ_2 in the energy range $0 - 2$ eV. Squares, experimental values [6]. Lines, calculated phase shifts using the pseudopotential shown in the figure.

Having found a potential for the e-Ne interaction which accurately reproduce the scattering properties of Ne atoms, we then applied the procedure of Ref. [17] to derive from it a (norm-conserving) pseudopotential to be used in our computer simulations. The $l = 0, 1, 2$ angular momentum components of the resulting (nonlocal) pseudopotential V_{ps}^l are shown in Fig. 2. In the inset we compare the scattering phase shifts calculated with this pseudopotential with the corresponding experimental values. Since in the energy range of interest here, up to a few hundred meV, the s-wave scattering dominates, we decided to keep only the $l = 0$ component, V_{ps}^s, of the pseudopotential shown in Fig. 2. The final electron-atom total potential to be used in the MD calculations is thus a local function of r, given by $V(\mathbf{r}) = \sum_I V_{\mathrm{ps}}^s(|\mathbf{r} - \mathbf{R}_I|)$.

IV. RESULTS AND DISCUSSION

Our MD calculations are performed on a periodically repeated system of one electron and N neon atoms, contained in a cubic cell of side $L = 36$ a.u. The electron wave function Ψ is expanded in plane waves on a mesh of $(30)^3$ points. Owing to the smoothness of the electron-Ne pseudopotential, a kinetic energy cutoff of 2.5 Ry (corresponding to ~ 1700 plane waves) was found sufficient to ensure a good convergence of the total energy of the system. We investigated a number of atomic densities, ranging from $\rho = 0.4 \times 10^{22}$ to 2.0×10^{22} cm^{-3} (corresponding to $N = 28$–138 atoms in our unit cell). In all our simulations the temperature of the system was kept

close to $\sim$ 48 K. Both temperature and densities were chosen to reproduce closely the experimental conditions [4, 5]. The equations of motion (3) were integrated by using the standard Verlet's algorithm, with a time step $\Delta t = 15$ a.u. and a fictitious mass $\mu = 300$ a.u. With these values the total energy of the system $E + K_I$ (see Sec. II) was conserved within $\sim 1 \times 10^{-4}$ during an entire MD run.

A typical run was as follows. For a chosen value of the gas density ρ, we obtained a starting atomic configuration via a preliminary (classical) MD simulation in the absence of the extra electron. Once a well-equilibrated neutral structure was obtained, we added the excess electron and computed the ground state for that initial atomic configuration. The system was then let to evolve freely under the action of the interatomic forces. We allowed the system to equilibrate for at least $\sim$ 2 ps prior to collect data for subsequent analysis. The lengths of the production runs following the equilibration runs were never less than $\sim$ 5 ps for any value of the Ne density investigated.

A number of quantities were monitored during the temporal evolution of the system, including the electron kinetic energy $E_{\rm kin} = -\frac{1}{2} < \Psi|\nabla^2|\Psi >$, the pseudopotential energy $E_{\rm ps} =< \Psi|\sum_I V^s_{\rm ps}(|\mathbf{r} - \mathbf{R}_I|)|\Psi >$, the total potential energy of the Ne atoms and the degree of localization of the electron in the unit cell.

In Fig. 3 we show the calculated values of the electronic energy terms $E_{\rm kin}$ and $E_{\rm ps}$ as a function of the Ne density. The values shown in the figure are actually temporal averages over the whole MD "production" run. Relative fluctuations in $E_{\rm ps}$ of $\sim$ 15% about its average value are found during the temporal evolution of the system after equilibration, while smaller fluctuations ($\sim$ 5%) in $E_{\rm kin}$ are observed.

From Fig. 3 it appears that as the density increases the total energy of the excess electron is dominated by the kinetic-energy term. However, a small but significant contribution comes from the pseudopotential energy term, especially at higher densities. Note that $E_{\rm ps}$ becomes more negative as the density increases. This is in contrast with the behavior of an excess electron in He [24], where the repulsive part of the potential dominates over the attractive polarization part, thus causing $E_{\rm ps}$ to increase with increasing He density.

Different behaviors of the excess electron are observed in our MD runs, depending on the density of neon. The analysis of the charge density shows that, while at low densities ($\rho < 1.0 \times 10^{22}\,{\rm cm}^{-3}$) the electron is always fairly delocalized all over the unit cell during the entire MD run, at higher densities it tends to localize.

In a finite system the concept of localization is not rigorously defined, but various practical indicators have been suggested. For instance, the participation ratio [25]

$$P = \left(\Omega \int_\Omega d\mathbf{r}|\Psi(\mathbf{r})|^4\right)^{-1} \tag{9}$$

gives a measure of the localization of the particle wave function in a finite volume Ω ($0 < P < 1$, where $P = 0$ and 1 for a perfectly localized and delocalized state, respectively).

In Fig. 4 we show the average participation ratio, calculated according to (9), at different densities. Note that although at low densities the participation ratio is close to 1, indicating a delocalized character of the electron state, at higher densities a sudden decrease is observed. We take this as an indication that a "localization transition" is likely to occur at $\rho \sim 1.5 \times 10^{22}\,{\rm cm}^{-3}$. This value should be compared with the experimental value $\rho \sim 1.4 \times 10^{22}\,{\rm cm}^{-3}$ where the transition from quasifree to localized behavior of the excess electrons is observed [5].

The nature of the electronic states in the high density region ($\rho > 1.5 \times 10^{22}\,{\rm cm}^{-3}$) is clarified by looking

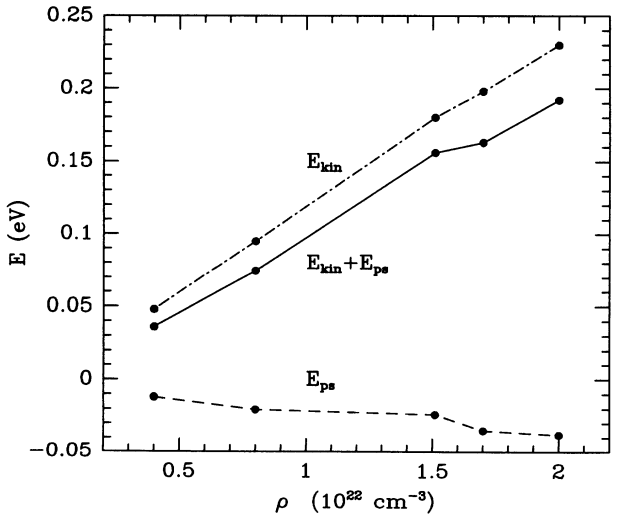

FIG. 3. Calculated electronic energies for different Ne densities. The values reported are averages taken over the whole MD "production" runs. The lines are only a guide to the eye.

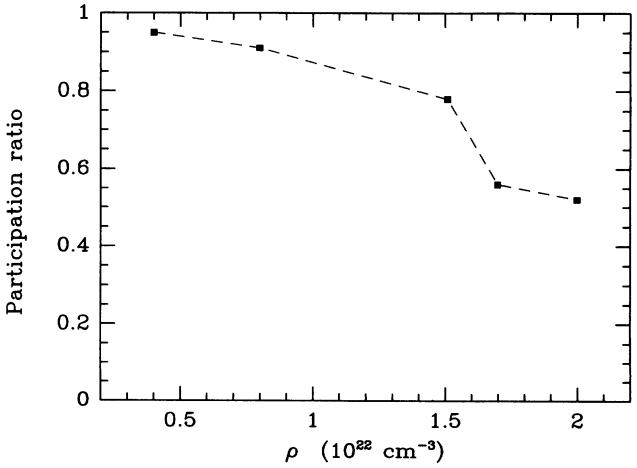

FIG. 4. Average participation ratio at different gas densities. The kink at $\rho \sim 1.6 \times 10^{22}$ suggests the onset of "localization." The dashed line is only meant to guide the eye.

at the electron charge density. A typical charge density plot is shown in the top panel of Fig. 5 (the figure refers to $\rho = 2.0 \times 10^{22}$ cm^{-3}) where the localized character of the electron state is evident. Moreover, a depletion of Ne atoms around the maximum in the electron density is clearly visible, indicating that self-trapping in a bubblelike cavity occurs.

To characterize the local fluid structure around this cavity, we computed the following correlation function:

$$g_{e\text{-Ne}}(r) = (4\pi r^2 \rho)^{-1} \left\langle \sum_I \delta(|\mathbf{R}_I - \mathbf{r}_e| - \mathbf{r}) \right\rangle, \qquad (10)$$

where the symbol $< \cdots >$ indicates a time average over the MD run. In the above formula r_e is the expectation value of the electron position $\mathbf{r}_e(t) \equiv < \Psi(t)|\mathbf{r}|\Psi(t) >$. Since periodic boundary conditions are used in our calculations, we computed $\mathbf{r}_e$ by using the following expression, which was proposed in Ref. [26] and found appropriate for a localized state in a periodic system:

$$< (\mathbf{r}_e)_\alpha(t) >= \frac{L}{2\pi} \mathrm{Im} \left(\ln \int_0^L e^{i2\pi r_\alpha / L} |\Psi(r,t)|^2 \, d\mathbf{r} \right) \qquad (\alpha = x, y, z). \quad (11)$$

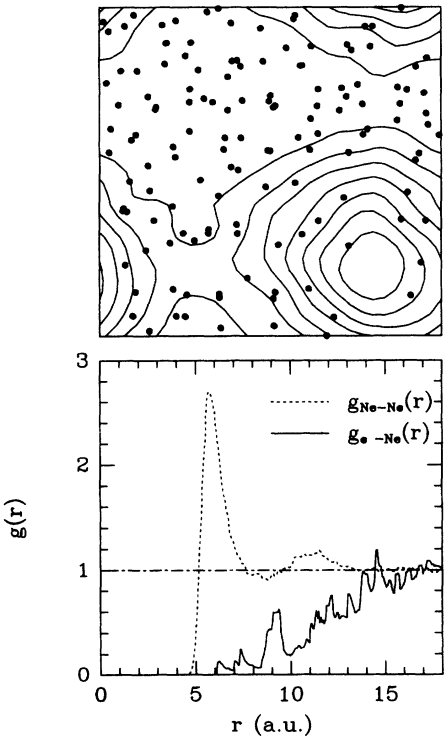

FIG. 5. Top panel: contour plot of the electron charge density (integrated along the sight line) for a typical atomic configuration at $\rho = 2.0 \times 10^{22}$ cm^{-3}. The dots indicate the Ne atom positions. Note the depletion of atoms around the center of the electron charge distribution. Bottom panel: Radial pair-correlation functions between Ne-Ne atoms (dashed line) and between the electron and the surrounding Ne atoms (solid line), at a density $\rho = 2.0 \times 10^{22}$ cm^{-3}.

From the behavior of the calculated $g_{e\text{-Ne}}(r)$, which is shown in the bottom panel of Fig. 5 with a solid line, one can see that Ne atoms are excluded from a region surrounding the electron and a well-defined cavity with a radius of $\sim$ 10–12 a.u. develops. Note that our estimate of the bubble radius is much smaller than the value $\sim$ 30 a.u. predicted at the same density by the model calculation of Ref. [7]. The time required to develop the bubble starting from the initial delocalized electronic state is roughly estimated from our simulations to be of the order of $\sim$ 3 ps at $\rho = 2.0 \times 10^{22}$ cm^{-3}. The energy gained by the electron in the localization process is rather small, being of the order of $\sim$ 0.06 eV. Very small fluctuations ($\sim$ 5%) in the kinetic energy of the electron are observed during the temporal evolution of the system after localization has occurred, thus showing that the variations in the size of the confining cavity are quite small.

For these localized states a low zero-field mobility is expected. The simplest way to calculate the excess electron mobility μ_e is to monitor the electron average position $< \mathbf{r}_e(t) >$, as given by (11), and to compute from it the correlation function [27]

$$< r_e^2(t) >= \lim_{T\to\infty} (1/T) \int_0^T [\, < \mathbf{r}_e(t+t') > - < \mathbf{r}_e(t') >]^2 dt'. \quad (12)$$

The long-time part of $< r_e^2(t) >$, which is shown in Fig. 6 with a solid line for the case $\rho = 2.0 \times 10^{22}$ cm^{-3}, is approximately linear, indicating a diffusive motion. Moreover, the nearly absence of fluctuations in $< r_e^2(t) >$ seems to indicate that the transport occurs in a smooth, dropletlike way. A diffusion coefficient D_e can be extracted from the asymptotic relation $< r_e^2(t) >\sim 6D_e t$, while the mobility μ_e can be estimated from D_e by means

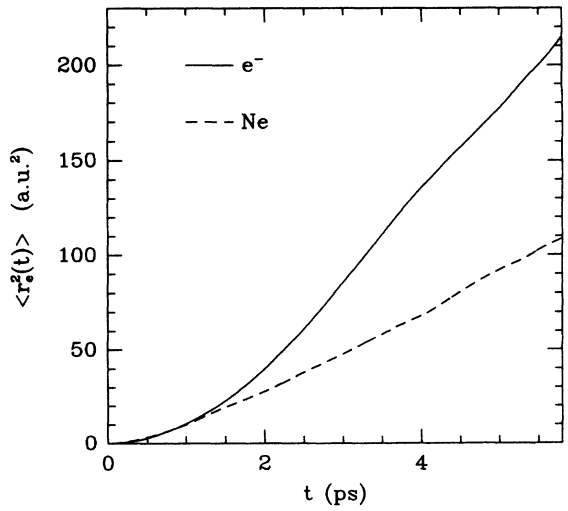

FIG. 6. Time dependence of (a) the electron mean-square displacement (solid line) as obtained from Eq. (12) in the text, and (b) the atomic rms displacement (dashed line), for the case $\rho = 2.0 \times 10^{22}$ cm^{-3}.

of the Einstein relation $\mu_e = eD_e/k_BT$. We remark that formula (11) applies in the case where the electron is localized to a certain extent in the unit cell. For the extended states which are found at lower densities ($\rho < 1.0 \times 10^{22}\,\mathrm{cm}^{-3}$), the above method does not apply, since the electron position (11) is in this case an ill-defined quantity. However, in the low-density quasifree regime the expression (1) from multiple-scattering theory is expected to be valid, once the zero-point energy ε_0 is calculated. In the present context the obvious choice for ε_0 is to take $\varepsilon_0 = E_{\mathrm{kin}} + E_{\mathrm{ps}}$, where E_{ps} and E_{kin} are the time-averaged values shown in Fig. 3. In the whole range of Ne densities investigated we are thus able to estimate the electron mobility from the analysis of our MD data.

We summarize our results in Fig. 7, where the calculated mobilities (full squares and diamonds) are compared with the available experimental data (open circles). The two values of the electron mobility at $\rho = 0.4$ and $0.8 \times 10^{22}\,\mathrm{cm}^{-3}$ are obtained using Eq. (1), while the point at $\rho = 2.0 \times 10^{22}\,\mathrm{cm}^{-3}$ is obtained from the calculated diffusion coefficient of the localized electron. With the open diamonds we also show the value of the mobility at $\rho = 2.0 \times 10^{22}\,\mathrm{cm}^{-3}$ as predicted using Eq. (1), i.e., assuming a quasifree behavior of the electron. The comparison between the full square and the diamond at $\rho = 2.0 \times 10^{22}\,\mathrm{cm}^{-3}$ shows the dramatic decrease in the mobility caused by the electron localization.

At $\rho = 1.7 \times 10^{22}\,\mathrm{cm}^{-3}$ we found difficult to extract a value for the diffusion coefficient D_e from the time dependence of $< r_e^2(t) >$. This could be due to the fact that at this density, which is close to the calculated transition density for localization, there is a coexistence of quasifree states with localized states, which makes problematic the use of (11) to calculate the electron position.

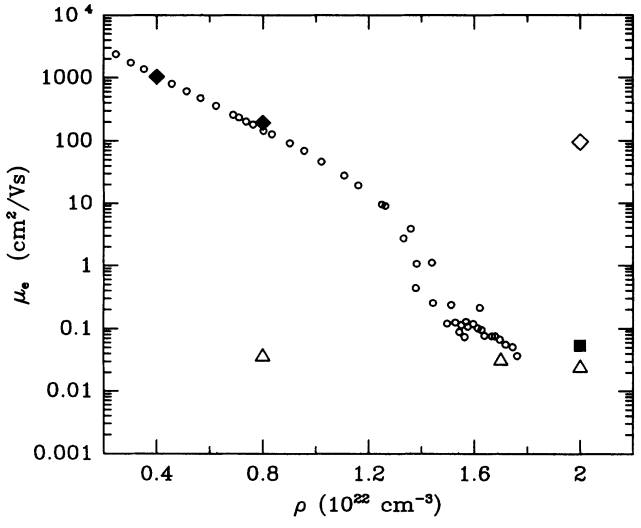

FIG. 7. Excess electron mobility in neon gas as a function of the gas density. Small open dots, experimental values [5]. Squares and diamonds, results of our MD calculations. The full diamonds shows the values of the mobility at low Ne densities as computed using Eq. (1), with ε_0 calculated from our MD runs (see text). The full square shows the mobility as computed from the time behavior of the electron mean-square displacement. For comparison, the value of the mobility obtained at the same density by using Eq. (1) is also shown with the open diamond. The open triangles correspond to calculated Ne mobilities due to self-diffusion.

It appears from Fig. 7, however, that the calculated mobility at the higher density is probably overestimated with respect to the experiments. Roughly speaking, a higher mobility means a smaller bubble radius R ($\mu_e \propto R^{-1}$, from Stokes's law). Thus this discrepancy could be due to a finite size effect since our unit cell is not able to accommodate very large bubbles, or it could also be due to spurious Ne-mediated interactions between the electron and its periodically repeated images.

In order to check for the effects of the finite size of our MD unit cell on the results presented so far, we performed additional calculations, at density $\rho = 1.7 \times 10^{22}\,\mathrm{cm}^{-3}$, using a cell with side $a = 45$ a.u., i.e., with a volume twice as large as that of the cell used previously. Due to the consequent increase in the computational burden, only MD runs of limited duration were performed, i.e., we followed the evolution of the system from the starting delocalized configuration until a well-defined bubblelike cavity is formed but we did not try to calculate the bubble diffusion coefficient. The time required for the bubble to form is found to be ~ 6 ps. As for the equilibrium properties of the localized electron, we find that the average electron energy $E_{\mathrm{ps}} + E_{\mathrm{kin}}$ is within 5% of the value obtained by using the smaller unit cell (see Fig. 3), while a bubble radius $R \sim 12$–15 a.u. is estimated from the electron-Ne correlation function. The latter value should be compared with $R \sim 10$–13 a.u. as obtained at the same Ne density using the smaller unit cell.

An *a posteriori* justification for our use of an adiabatic dynamics scheme is provided by the calculation of the electronic excitation spectrum. We have calculated the electronic excited states for a number of selected atomic configurations taken from our MD trajectories, in order to extract an average excitation spectrum. For instance, in the case $\rho = 2.0 \times 10^{22}\,\mathrm{cm}^{-3}$ we found a substantial energy gap $E_g \sim 0.35\,\mathrm{eV} \sim 75 k_BT$ between the ground state and the first excited state, all the higher excited states being more closely spaced in energy. We are thus in the conditions where the adiabatic separation between the electronic and atomic motion is expected to be valid.

We note finally that during our MD simulations we never observed any attempt of the system to make (adiabatic) hopping transitions, where the electron, initially localized in a cavity of the fluid, is able to tunnel into an empty cavity created by spontaneous fluctuations in the gas density. Moreover, due to the large energy gap, other nonadiabatic processes which could contribute to the diffusion of the electron through excitation into higher energy delocalized states are expected to contribute negligibly to transport.

V. CONCLUSIONS

In summary, we have calculated a number of properties of an excess electron in Ne gas in a wide range of densities, using molecular dynamics with parameter-free

interparticle potentials. As the Ne density increases, we find evidence of a transition from quasifree to localized electronic states where the electron is self-trapped in a bubblelike cavity in the fluid. We have been able to elucidate the nature and the diffusion process of the localized states that occur at higher densities. The comparison with recent experimental measurements of excess electron mobilities in Ne is satisfactory in the whole range of densities investigated. The effect of the finite size of the MD supercell on the energy of the localized electron and on the bubble radius is also investigated.

ACKNOWLEDGMENTS

We are grateful to A. Selloni, M. Santini, F. Borghesani, and P. Scatturin for helpful discussions. This work was supported by Ministero della Ricerca Scientifica through Consorzio Interuniversitario di Struttura della Materia–INFM, Unitá di Padova.

[1] See, for instance, *Electrons in Fluids*, edited by J. Jortner and N.R. Kestner (Springer, Berlin, 1973); J. Phys. Chem. **88**, 3699 (1984), Colloque Weyl VI.

[2] The basic physics of self-trapping of electrons in simple fluids has been reviewed recently by J.P. Hernandez, Rev. Mod. Phys. **63**, 675 (1991).

[3] J.L. Levine and T.M. Sanders, Phys. Rev. Lett. **8**, 159 (1962); T.P. Eggarter and M.H. Cohen, *ibid.* **27**, 129 (1971).

[4] A.F. Borghesani, L. Bruschi, M. Santini, and G. Torzo, Phys. Lett. **108A**, 255 (1985); Phys. Rev. A **37**, 4828 (1988).

[5] A.F. Borghesani and M. Santini, Phys. Rev. A **42**, 7377 (1990).

[6] T.F. O'Malley and R.W. Crompton, J. Phys. B **13**, 3451 (1980).

[7] J.P. Hernandez and L.W. Martin, Phys. Rev. B **43**, 4568 (1991).

[8] See, for instance, *Computer Modelling of Fluids, Polymers and Solids*, edited by C.R.A. Catlow, S.C. Parker, and M.P. Allen (Kluwer Academic, Dordrecht, 1990).

[9] R. Car and M. Parrinello, Phys. Rev. Lett. **55**, 2471 (1985).

[10] *Simple Molecular Systems at Very High Density*, Vol. 186 of *NATO Advanced Study Institute, Series B: Physics*, edited by A. Polian, P. Loubeyre, and N. Boccara (Plenum, New York, 1988), Vol. 186, p. 455.

[11] K.T. Tang and J.P. Toennies, J. Chem. Phys. **80**, 3725 (1984)

[12] K.T. Tang and J.P. Toennies, Z. Phys. D **1**, 91 (1986).

[13] L.A. de Graaf and B. Mozer, J. Chem. Phys. **55**, 4967 (1971).

[14] H.J. Raveche and R.D. Mountain, J. Chem. Phys. **57**, 3987 (1972).

[15] D. Thirumalai, R.W. Hall, and B.J. Berne, J. Chem. Phys. **81**, 2523 (1984).

[16] G.B. Bachelet, D.R. Hamann, and M. Schluter, Phys. Rev. B **26**, 4199 (1982).

[17] D.R. Hamann, Phys. Rev. B **40**, 2980 (1989).

[18] H.P. Saha, Phys. Rev. Lett. **65**, 2003 (1990).

[19] J.K. O'Connell and N.F. Lane, Phys. Rev. A **27**, 1893 (1983).

[20] E. Clementi and C. Roetti, At. Data Nucl. Data Tables **14**, 177 (1974).

[21] S. Hara, J. Phys. Soc. Jpn. **22**, 710 (1967).

[22] J.P. Perdew and A. Zunger, Phys. Rev. B **23**, 5048 (1981).

[23] D.M. Ceperley and B.J. Alder, Phys. Rev. Lett. **45**, 566 (1980).

[24] D.F. Coker, B.J. Berne, and D. Thirumalai, J. Chem. Phys. **86**, 5689 (1987).

[25] R.J. Bell and P. Dean, Discuss. Faraday Soc. **50**, 55 (1970).

[26] A. Selloni, P. Carnevali, R. Car, and M. Parrinello, Phys. Rev. Lett. **59**, 823 (1987).

[27] E. Fois, A. Selloni, M. Parrinello, and R. Car, J. Phys. Chem. **92**, 3268 (1988).